

TOP detector for particle identification at Belle IIEzio Torassa
(On behalf of the Belle II TOP group)*INFN Sezione di Padova*
35131 Padova, Italy
*ezio.torassa@pd.infn.it*Received Day Month Year
Revised Day Month Year

The Time-Of-Propagation (TOP) counter is a ring-imaging Cherenkov detector designed to identify the charged hadrons in the barrel region of the Belle II detector. The Belle II experiment collected data delivered by the SuperKEKB accelerator from March 2019 to June 2022. After the first run period (Run1) a long shutdown (LS1) was dedicated to implement several accelerator and detector upgrades. The most important upgrade was the completion of the vertex detector. The second collision period (Run2), started in January 2024. The components of the TOP detector and the performance during the Run1 will be reported, the detector upgrade during LS1 and the future upgrades will be described.

Keywords: TOP; particle identification; Belle II.

PACS numbers:

1. Introduction

The TOP detector replaced the Aerogel Cherenkov Counter of the Belle experiment, it consists of 16 modules made by quartz bar radiators read-out by Micro-Channel Plate Photomultipliers (MCP-PMTs). The TOP modules are arranged in the central region of the Belle II detector¹ between the Central Drift Chamber (CDC) and the Electromagnetic Calorimeter (ECL) (Fig. 1, left) . The quartz bars act as Cherenkov radiator and photon collectors. Thanks to the high average refractive index, the Cherenkov radiation remains trapped inside the bars and propagates to the photodetectors through internal reflection. Different hadrons crossing the quartz bar with the same angle have Cherenkov photons emitted at different angles, they arrive at the photodetector plane in different channels and at different times (Fig. 1, right). The time of arrival is measured relative to the e^+e^- collision time, it includes the time-of-flight (Tof) of the particle and the time-of-propagation (Top) of photons:

$$K/\pi \text{ Tof difference} \sim 50 \text{ ps}/m \quad K/\pi \text{ Tof difference} \sim 75 \text{ ps}/m$$

$$\text{PID sensitivity} \propto \frac{\Delta \text{ Tof} + \Delta \text{ Top}}{\sigma_{\text{Time}}} \sqrt{N_\gamma}$$

2 *E. Torassa*

The number of photons N_γ is 20-30 depending to the track angle. Radius of the TOP cylinder is 1.2 m therefore $\Delta T_{of} + \Delta T_{op}$ is on the order of 100 ps, it follows the requirement of the time resolution $\sigma_{Time} \leq 100$ ps to keep a good PID sensitivity. The arrival position and time of photons are measured with a 2D segmentation of 16 channels per in^2 and a time resolution better than 100 ps. For every track the probability to be a specific particle is estimated by comparing the resulting space-time distribution of the arriving photons with the probability density function expected for this particle hypothesis. The particle identification capability has been tested by selecting pure samples of pions, kaons and protons tagged reconstructing D^* , K_S and Λ particles decays.

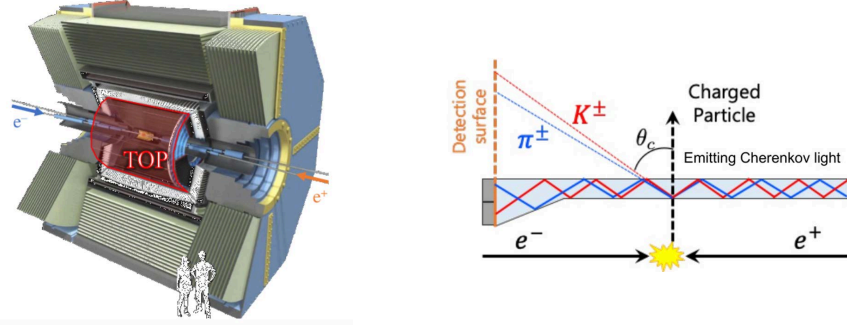


Fig. 1. The Belle II and the TOP detectors (left). Cherenkov photons emitted at different angles by pion and kaon hadrons (right).

The TOP detector was constructed within the original time schedule, the installation was completed in May 2016. The drawback was the use of a small fraction of the latest generation of photomultipliers having long lifetime. Half of the MCP-PMTs have been replaced during LS1, the others will be replaced during the next long shutdown.

2. TOP detector

The key elements of the TOP detector are described in the following.

2.1. Cherenkov radiator and light guide

The Cherenkov radiator and light guide elements are shown in Fig. 2 for a single TOP module. Four parts are glued together: two fused silica bars each of dimension $(1250 \times 450 \times 20)$ mm³ acting as the Cherenkov radiator, a mirror located in the forward region with dimension $(100 \times 450 \times 20)$ mm³ and a prism that couples the bar to an array of MCP-PMTs in the backward region with dimension $(100 \times 456 \times 20-51)$ mm³. The high refractive index of the radiator ($n=1.44$ for $\lambda = 405$ nm) with high geometrical precision, bulk transmittance and surface reflectance (Table 1) minimize the loss of photons during propagation.²

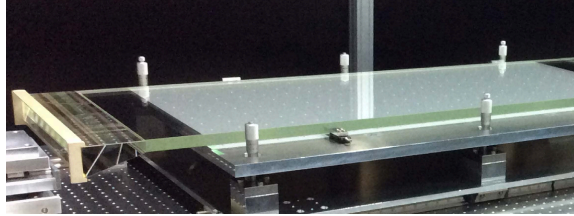


Fig. 2. Cherenkov radiator and light guide elements for a single TOP module.

Table 1. Manufacturing specifications of the quartz bars.

Quartz properties	Requirements
Flatness	$< 6.3 \mu\text{m}$
Perpendicularity	$< 20 \text{ arcsec}$
Parallelism	$< 4 \text{ arcsec}$
Roughness	$< 0.5 \text{ nm (RMS)}$
Bulk transmittance	$> 98\% / m$
Surface reflectance	$> 99.9\% / \text{reflection}$

2.2. MCP-PMT photodetectors

The expansion volume of the quartz radiator bar is coupled in the back side with an array of two rows of MCP-PMTs, in total 32 photodetectors per module. Each MCP-PMT is square-shaped, has an effective area of $(23 \times 23) \text{ mm}^2$ and is segmented into 16 channels (Fig. 3, left). The 16 TOP modules have in total 8192 channels. The photoelectrons are multiplied inside two microchannel planes, each plane is $400 \mu\text{m}$ thick, each channel has $10 \mu\text{m}$ diameter. Channels are tilted to prevent electrons from passing through the holes without multiplication process (Fig. 3, right). The multiplication in the short path makes the transit time spread less than 50 ps .



Fig. 3. The Hamamatsu R10754-07-M16(N) microchannel plate photomultiplier tube (left). Two microchannel plates with angled channels (right).

During the mass production, three types of MCP-PMTs have been developed to improve the lifetime of the photocathode.³

- (1) Conventional MCP-PMT

4 *E. Torassa*

In the manufacturing process of conventional MCP-PMT a lead glass disk with holes is built with thermal and etching processes.⁴ This lead glass capillary array is then heated in presence of hydrogen, which chemically reduces the surfaces of holes, leaving a resistive and emissive surface that is effective for electron amplification.

(2) Atomic layer deposition ALD MCP-PMT

This new technology does not use material containing lead which is a harmful element restricted by the RoHS (restriction of hazardous substances) directive of the European Union. The new glass capillary array is coated using the ALD technology with a resistive film and with a secondary electron multiplier film with high uniformity in each micro channel.

(3) Life-extended ALD MCP-PMT

Each components of of the MCP-PMT get an optimized backing to reduce the trapped ions. The residual ions can be released during the development of the electron avalanche and can reduce the lifetime of the photocathode.

Based on the development of the MCP-PMT technology during the TOP detector construction, 44% of the installed PMTs were conventional MCP-PMTs, 43% were ALD MCP-PMTs and 13% were life-extended ALD MCP-PMTs.

2.3. *Front-end readout electronics*

The TOP front-end electronics are required to read out the signals of all 8192 MCP-PMT channels in the whole TOP system with a global timing resolution of better than 100 ps at a nominal trigger rate of up to 30 kHz. This is achieved by employing specially designed 2.7 GHz wave-form sampling electronics. The TOP readout is organized as an ensemble of 4 boardstacks per module (Fig. 4). Every boardstack contains 4 ASIC carrier boards and a single Standard Control Read-Out data (SCROD). Every carrier board contains 4 Ice Ray Sampler version X (IRSX) chips with 8 channels/chip.⁵

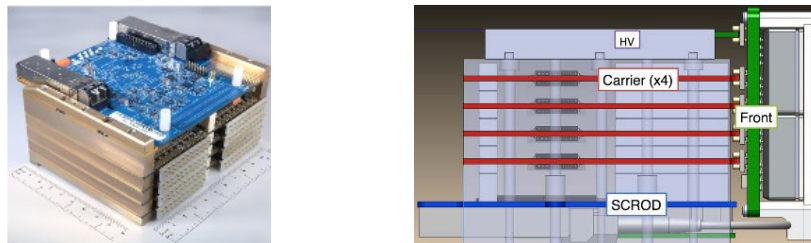


Fig. 4. TOP boardstack consisting of one SCROD board, four AISC boards and one HV supply module.

For every channel an internal trigger system based on a fixed threshold marks regions of interest. Every region of interest has a length of 32 samples, about 12 ns.

The SCROD extracts the timing of photon pulses for every channel and transfer the data to the Belle II DAQ system.

2.4. Laser calibration system

The laser calibration system was designed to calibrate the time differences between the 8192 channels of the TOP detector with a resolution better than 100 ps .⁶ To achieve this, it is necessary to reach all channels of all photodetectors with a single photon source while maintaining a time resolution of few tens of picoseconds in each step. To inject the calibration light in the box containing the quartz prism, the number and size of holes should be as minimal as possible to avoid loss of Cherenkov light. Simulation studies shown the best optical and mechanical solution was to inject the light in 9 holes with steps of 50.7 mm with a vertical angle of 15° and light numerical aperture $0.5 < NA < 0.6$ (Fig. 5, right).

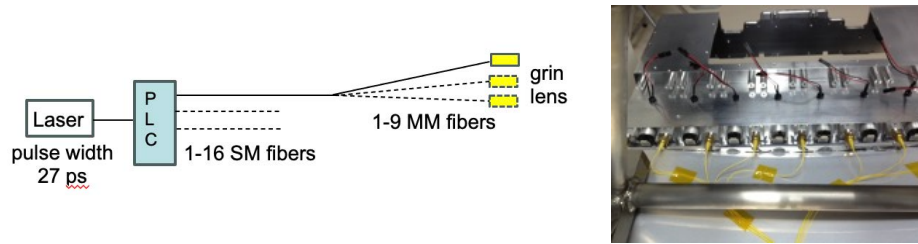


Fig. 5. Scheme of the laser calibration system (left). Picture of the prism box with the laser calibration fibers installed.

The calibration light source is provided by a PiL040X pulsed laser diode with 405 nm of wavelength, pulse width less than 27 ps , and peak power of 300 mW . A Planar Lightwave Circuit (PLC High Power Splitter from PPI Inc.) followed by 30 m long single-mode (SM) fibers, demultiplex the light for the 16 TOP modules. For every module a multi-mode (MM) fiber bundle split the light to the 9 light entries. For every bundle the end side of every fiber is coupled with a grin lens (Selfoc-SLH) with a nominal $NA = 0.6$ (Fig. 5, left).

3. Time calibration

The time calibration is performed in four steps:⁷

(1) Time Base Calibration

Each channel of the IRSX ASIC consists 128 sampling windows, the analog information are stored in 32k cells and readout by 64 Wilkinson ADCs. The different sampling windows have different delays to be precisely calibrated. A double peak pulse with fixed time difference of 22 ns is injected in the electronics. In order to cover all the 128 elements the double pulse is not synchronized

6 *E. Torassa*

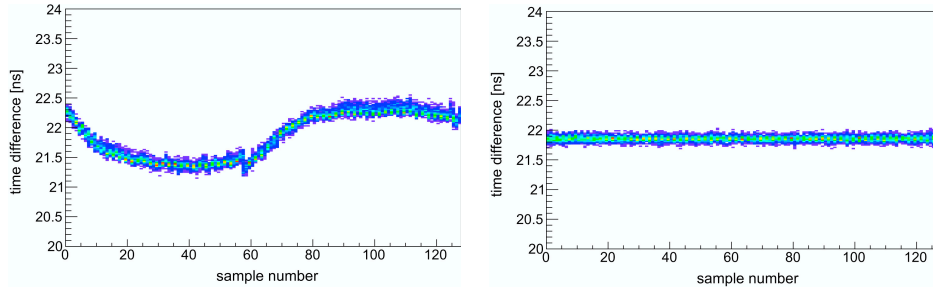


Fig. 6. Time difference of two calibration pulses as a function of sample number before (left) and after (right) the time base calibration.

with the accelerator clock. Figure 6 shows the measurement of the time difference as a function of the sample number. Time fluctuations up of 1 ns have been reduced after the time base calibration to 42 ps of r.m.s.

(2) Time assignment of channels within a module

The time alignment of channels within a module is performed with the laser calibration system. The small time jitter of the laser allows the different time response of the 512 channels of each module to be measured. However single channels can receive light directly or after reflections inside the prism, they can also be illuminated by two fibers. A simple method is to align the average of the time distribution in each channel. Figure 7 shows the times for the 128 channel in a single boardstack before and after the alignment, with respect to a common time related to the laser trigger. A more precise method with time offset fit was implemented, it takes into account the different intensities after reflections and the possible propagation times taken from Monte Carlo.

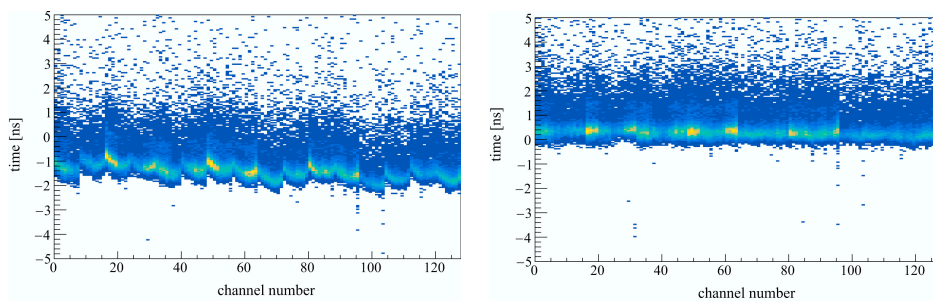


Fig. 7. Times for the 128 channel in a single boardstack before (left) and after (right) alignment.

(3) Time alignment of modules

The 16 TOP modules are aligned together within few tens of ps using cosmic rays and dimuons from collision data. The same kind of data can be used also for the geometrical alignment after the summer and winter stops or after an earthquake.

(4) Alignment relative to collision time

The global T_0 with respect to the RF accelerator clock is measured using dimuons from collision data.

4. TOP detector performance

Particle identification performance is estimated with Likelihood ratio by comparing the assumed particle with respect to the sum of alternative options. Different choices are possible for this ratio:

$$R[K/\pi] = \frac{\mathcal{L}_K}{\mathcal{L}_K + \mathcal{L}_\pi} \quad p[h] = \frac{\mathcal{L}_h}{\sum_{h'} \mathcal{L}_{h'}} \quad \mathcal{L}_h = \mathcal{L}_h^{TOP}$$

(binary PID) (global PID) (TOP only)

The PID performance of the TOP detector shown in Figure 8 was obtained by varying the $K - \pi$ binary ratio. Two data-set periods are reported and compared with the Monte Carlo expectation. The performance is stable in time, the difference with respect to Monte Carlo shows the simulation of the detector can still be improved. The identification efficiency for Kaons selected with $R(K/\pi) > 0.5$ and

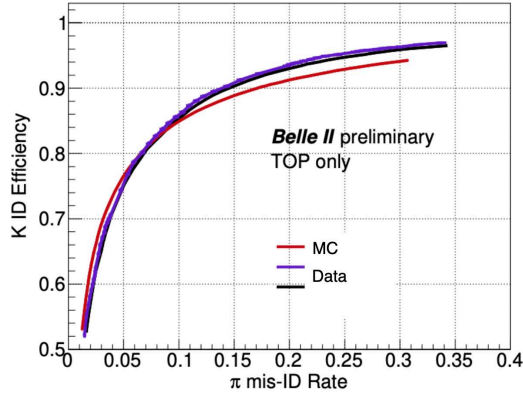


Fig. 8. K identification efficiency as a function of the pion mis-identification rate for two data-set periods (blue and grey) and for the Monte Carlo (red).

the mis-identification of pions are shown in Figure 9 in bins of momentum using all sub-detectors (left) or TOP only (right) information. Kaons and pions have been tagged from the $D^{*+} \rightarrow D^0[K^-\pi^+]\pi^+$ decay. The efficiency is about 85% and almost uniform in all the TOP slots. Machine learning approach is under study where weights used to combine PID information are not static but function of charge of the track and its kinematics.

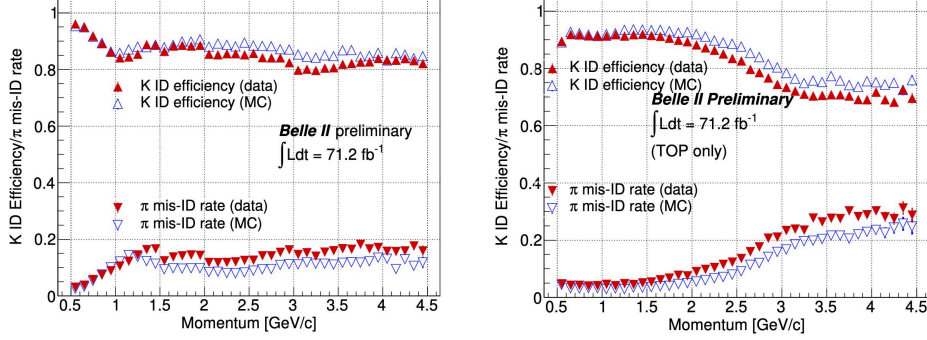
8 *E. Torassa*


Fig. 9. Kaon efficiency as a function of momentum in the laboratory frame for the PID criterion $R(K/\pi) > 0.5$ using all sub-detectors (left) or TOP only (right).

5. TOP detector upgrade

After the first run period 4 boardstacks were dead, 10 boardstacks were showing small issues during operation. The TOP detector had in total about 600-700 dead channels out of 8192. All the boardstacks and electronics boards showing problems have been replaced during LS1. The accumulated charge of the photodetectors was between $0.2 C/cm^2$ and $0.3 C/cm^2$ depending to the slot and to the photodetector type. The lifetime of MCP-PMTs is defined as the accumulated charge which has the effect of reducing the photocathode quantum efficiency (QE) to 80%. The lifetime measured in laboratory is $1.1 C/cm^2$ in average for the conventional MCP-PMTs, $10.4 C/cm^2$ in average for the ALD MCP-PMTs and $> 10.4 C/cm^2$ for the extended-lifetime ALD MCP-PMTs. Considering the large fluctuation of these measurement (from 0.3 to $1.7 C/cm^2$ for the conventional type) and the expected increase of luminosity and background, the conventional MCP-PMTs have been replaced even though the QE was not expect to be significantly degraded in average. The removed MCP-PMTs have been tested in laboratory, the measured QE shown a faster degradation than expected. The possible explanation is the heating of the photodetectors due to electronics. The hypothesis was verified by measuring the quantum efficiency degradation at different environmental temperatures, a faster degradation was found for higher temperatures. Figure 10 shows the distribution of the different type of MCP-PMT before LS1, after LS1 and the plan for the next long shutdown LS2. The production of the missing life-extended MCP-PMTs is ongoing, 150 new MCP-PMTs have been already delivered or ordered out of 220. The ALD MCP-PMTs have been moved from the top to the bottom slots to have a backup option of early replacement during the annual summer break in case of faster-than-expected QE degradation. Upgraded electronics with less power consumption and more compact design is being considered as well as further lifetime improvements for MCP-PMTs or new type of photodetectors like SiPMs.

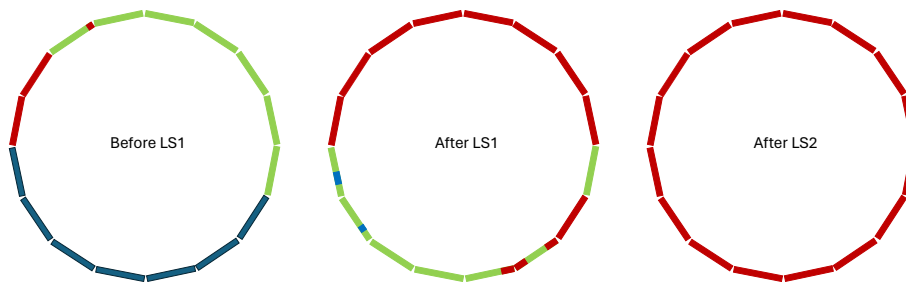


Fig. 10. Distribution of conventional MCP-PMTs (blue), ALD MCP-PMTs (green) and life-extended ALD MCP-PMTs (red) inside the 16 modules of the TOP detector before LS1, after LS1, and after the next long shutdown.

6. Conclusions

TOP is a new concept of a compact Cherenkov detector for particle identification which relies on multichannel long-lifetime MCP-PMTs for the precise measurement of the arrival position and time of individual photons. The installation of the TOP detector has been completed in May 2016, it is successfully operating since the start of physics collisions in March 2019. TOP only binary PID gives 85% of Kaon identification efficiency with 10% of pion mis-identification rate. After LS1 the fraction of active channels increased from 91 – 93% to 99.5%. The TOP upgrade program for the LS2 shutdown is well underway with 68% of missing life-extended MCP-PMTs already delivered or ordered.

Acknowledgements

This work was supported by the following European Union’s funding sources: Horizon 2020 Marie Skłodowska-Curie RISE project JENNIFER2 grant agreement No. 82207, Horizon 2020 Research and Innovation project AIDAinnova grant agreement No. 101004761.

References

1. Belle II Collaboration, Belle II technical design report, arXiv:1011.0352 (2010).
2. K. Suzuki, *Nucl. Instrum. Methods Phys. Res. A* **876**, 252 (2017).
3. K. Inami, *Nucl. Instrum. Methods Phys. Res. A* **936**, 556 (2019).
4. J. L. Wiza, *Nuclear Instruments and Methods* **162**, 587 (1979).
5. D. Kotchetkov et al., *Nucl. Instrum. Methods Phys. Res. A* **941**, 162342 (2019).
6. U. Tamponi, *Nucl. Instrum. Methods Phys. Res. A* **876**, 59 (2017).
7. M. Starič, *Nucl. Instrum. Methods Phys. Res. A* **876**, 260 (2017).
8. S. Sandilya et al., *J. Phys.: Conf. Ser.* **2374** 012107 (2022).